Journal of Materials Chemistry C

Accepted Manuscript

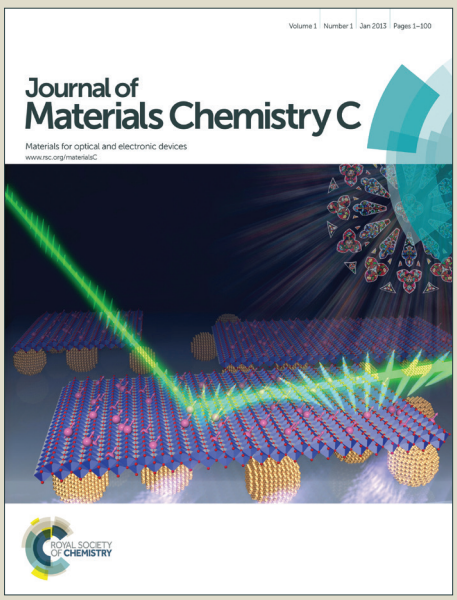

ROYAL SOCIETY OF CHEMISTRY

www.rsc.org/materialsC

Scalable approach for the realization of garland shaped 3D assembly of CuTCNQ nanorods: efficient electron emitter

Shreyasi Pal[a], Soumen Maiti[a], Uday Narayan Maiti[b], and Kalyan Kumar Chattopadhyay[a*]

[a]Thin Films and Nanoscience Laboratory, Department of Physics, Jadavpur University, Kolkata 700032, India, [b] KAIST, South Korea.

Corresponding Author: Email: kalyan_chattopadhyay@yahoo.com

Abstract:

Going beyond the conventional presentation of CuTCNQ nanostructures over 2-dimensional Cu /Cu coated substrate, in the current work, 3-dimensional back bone of metallic Cu nanowire was used to materialize garland shaped hierarchical nanoforms. Simplicity and scalable amount of high quality products yield are the hallmarks of the current synthesis procedure, which in retrospective offers a brilliant contrast to the existing severe lack of adequate protocols for synthesizing CuTCNQ nanostructure in bulk. In the present approach, gradual consumption of Cu in acetonitrile solution during prolonged intervals is found to be responsible for triggering structural variances. A possible growth mechanism, substantiated by FESEM and XRD analysis, and based on temporal morphology evolution was proposed also. The optimized hierarchy, armed with emission beneficial large number of emitters and appreciable inter tip separation, are found to exhibit high field emission performance with low turn on and threshold field values (2.69 and 6.11 Vμm^{-1} respectively). Moreover via electrostatic field distribution calculation using 'ANSYS Electromagnetic' software, the experimental electron emission result was verified. This facile strategy may well pave the way for practical realization of other charge

transfer complex nanostructures, and on its own, warrants their potential usage as humidity sensors, photo-detector and photocatalyst etc.

Introduction:

Assembly and integration of 1-dimensional nanostructures into more complex geometry, especially in hierarchically intricate superstructures, is of paramount interest as they not only inhibit the analogous features of the single nano-building blocks, but also bestow improved and unusual aspects by combining those singularities. Moreover, elaboration of these 3-dimensional arrangements provides further help to utilize diverse material functionalities through profound morphology control. Besides creative designing, these hierarchical assemblies with multiple components also pervade the contemporary nanostructure based electronic, optoelectronic application arena, owing to their superior and some unique device performances.[1-3] Amongst various potential aspects of field emission, field assisted electron emission from these complex hierarchy is a topic that is persistently investigated for last decade where the documented reports were primarily confined to carbon based inorganic materials or other oxide based inorganic materials.[2,4,5] But high-temperature processing, costly deposition equipment and complex synthesis protocol associated with these nanoforms managed to cast a bleak shadow over their potential commercial usage. Additionally, compared to the abundance of reports on inorganic hierarchy, documentation on organic materials is very much sparse. Thus organic material based higher dimensional complex nanoforms prevail over their lower dimensional counterparts, and their generation via facile, low budgetary and environment benign approaches garner great significance from both research and practical application point of views.

Amongst organic materials, 7,7,8,8-tetracyanoquinodimethane (TCNQ) based charge transfer salts, especially CuTCNQ have stimulated great enthusiasm owing to their peculiar electrical and optical features.[6-12] Between two polymorphs of CuTCNQ, highly conductive phase I,[13] having greater number of charge carriers, registered their potential worth in functional nanoscale devices. Moreover, emergence of CuTCNQ, which endow very low turn on field owing to their low work function, helped to draw substantial research interests on organic nanostructure based cold cathode emitters.[14-17] Additionally, low cost fabrication techniques also help to provide further boosts to their usage perspective. To enhance the FE performances, prior attempts were made to modify the CuTCNQ nanostructures morphology. However, till now, implementations of most of these protocols only did succeed to realize CuTCNQ nanostructures over conventional 2-dimensional substrates.[14-18] Development of CuTCNQ hierarchical architectures with multiple components may be a possible route to enrich the emission performances where the applied electric field can be boosted up by its branched geometry and thereby opening the possibility of a new breed of low operating voltage field-emitters.

Herein, a simple synthesis protocol was adopted for the preparation of scalable amount CuTCNQ nano-garlands, in which going beyond the simple metallic Cu foil or Cu coated substrates, we have synthesized the charge transfer complexes over chemically synthesized Cu nanowire backbones. The growth mechanism was investigated in detail via monitoring the temporal dependence on morphology. Along with the exploration of the possible growth behaviors, these CuTCNQ hierarchies were also rigorously tested for potential field electron emission applications. Owing to their emission favorable geometry, these hierarchical nanoforms were found to exhibit outstanding electron-emission activity with high emission current as well as low field values (turn on and threshold). Synthesis of nanostructure in bulk is inevitable for many

applications like photocatalysis, composite, printed electronics where mass sample production in powder form is required. Thus the application window of our synthesis protocol is not restricted to generate efficient field emitter but they are equally appealing for aforementioned areas of interest.

Experimental:

Synthesis of Cu nanowires:

Initially, Cu nanowire was prepared by a hydrothermal technique analogous to the procedure described by Kevin et al.[19] In brief; 0.53 g octadecylamine and 0.13 g anhydrous copper (II) chloride were added to 80 ml D.I. water and was mixed by ultrasonication until a smooth light blue emulsion was formed. Then the emulsion was transferred to a 100 ml autoclave and was maintained at 160 $^{\circ}$C for 3 days. After the reaction span, it was allowed to cool down to room temperature naturally. Thick sheets comprising of Cu nanowires were found to settle down at the bottom of the autoclave which was then collected and washed with copious amount of D.I water prior to drying in vacuum at room temperature.

Synthesis of CuTCNQ hierarchical structure:

As formed Cu nanowires were then immersed in 5 mM TCNQ dissolved in acetonitrile solution following which the reddish colored Cu nanowires turned bluish very rapidly. After a reaction span of 2 minutes, the sample was washed five times with D.I. water and was dried in vacuum at 45 $^{\circ}$C overnight.

Furthermore, additional time resolved experiments were also undertaken to explore the morphological variances and thereby the mechanism behind structural evolution of CuTCNQ

hierarchies in minute detail. Henceforth we will denote the samples corresponding to 30 sec, 2 min, 5 min, 30 min and 60 min reaction span as T0, T2, T5, T30 and T60 respectively.

Characterization: Please see the supporting information†.

Results & Discussion:

Low magnification FESEM image and digital image (Supporting information S1a†) evidently manifests high yield exceptionally long (~100 µm) Cu nanowires. Zoom in view (fig 1a) of these nanowires discloses smoothness of surface and near uniform diameters in the range 100~150 nm. Ambient conditioned treatment in acetonitrile and TCNQ mixture was found to induce complete structural transformation of these nanowires as numerous CuTCNQ nanorods were found to form hierarchical nanostructures where the visible signature of primary Cu nanowire was totally absent. For small growth time (T2) the as grown hierarchy is shown in figure 1b where the nanorods are quite separated from each other and the average length is ~350 nm. For higher growth time (T5) the CuTCNQ nanorods become more compact to form garland like hierarchical architecture (figure 1c). Pictorial resembles with actual garland and dimensional aspects are obvious from digital image (figure 1c inset) and FESEM image (figure 1d) respectively. Average lengths of the CuTCNQ nanorods were found to be ~550 nm and their top diameter were found be ~60 nm. Additionally, notable morphological uniformity of the hierarchical products in low magnification images (figure 1c and S1b†) highlights large scale formation.

Further characterization of Cu nanowire and hierarchical samples were executed by TEM to get into the exact morphology. Low magnification TEM images of numerous Cu nanowires along with high magnification view of a single nanowire (shown in figure **S**2a† and its inset) reveal the smooth side surfaces of the nanowires and typical diameter which is in a range of 100 to 150 nm.

Several CuTCNQ nanorods radiating in outward direction for both samples (T2 and T5) are prominent from the corresponding TEM images (figure S2b† and its inset). From these figures the higher compactness of the nanorods in the T5 is also visible. Finally, selected area electron diffraction (SAED) pattern shown in figure S2b† (lower inset), manifests the crystallinity of the CuTCNQ hierarchy (T5).

For evaluating phase structure of Cu nanowire and CuTCNQ hierarchy, x-ray diffraction was utilized and the corresponding spectra are presented in figure 2a. The strong peak (*) in the pattern (Cu nanowire) is attributed to Cu which commensurate well with JCPDS file (04-0836). No trace of other oxide related peaks (CuO/Cu_2O) confirm high phase purity. Analysis of low-index diffraction peaks in the spectra associated to T2 and nano-garland (T5) confirm CuTCNQ phase I structure with a tetragonal unit cell of a = 3.89 Å, b = 11.26 Å, and c = 11.27 Å.[18,20]

XPS spectroscopy was used to analyze the surface composition of the CuTCNQ nano-garland (T5). In figure 2b, two characteristics peaks of Cu 2p, comprising of Cu $2p_{3/2}$ and Cu $2p_{1/2}$ could be observed at 932.2 eV and 952 eV respectively and commensurate well with the presence of Cu^{+}.[21] Significantly, signature of no other shoulder or satellite peaks in the spectrum (due to Cu/ Cu^{2+}) confirms high purity of the synthesized samples. XPS spectra for N1s regions peaked at 399 eV as single feature indicate only one valence state of TCNQ (figure 2c).

To determine the oxidation and reduction states of the acceptors and their CT complexes, FTIR spectra was recorded. FTIR spectra of the CuTCNQ nano-garland (T5) (figure 3a) provide the evidence for bonding between Cu and TCNQ. When compared with the same for pure TCNQ powder, FTIR spectra of CuTCNQ shows obvious changes. CuTCNQ shows strong absorption band at 2198 cm^{-1} (C≡N stretching mode),[14] whereas the band corresponding to the same

stretching mode is found to appear at 2224 cm^{-1} for TCNQ.[22] The above could be accounted to and explained by coordination of C≡N groups of TCNQ with metallic copper ions. Weak absorption bands at 1577 and 1506 cm^{-1} corresponding to C=C ring stretching[23] for CuTCNQ nano-garland were also observed to be shifted in comparison to pristine TCNQ (1543 cm^{-1}).[22] These results indicate that formation of different oxidation states of TCNQ in CuTCNQ than pristine TCNQ. Furthermore, the band related to C=C–H bending at 826 cm^{-1} in CuTCNQ[23] was also found to shift from 860 cm^{-1} for neutral TCNQ[22] which is consistent with the sole presence of $TCNQ^{-}$.

Degree of Charge transfer between donor (metal) and acceptor was further assessed from Raman spectrum comparison between pristine TCNQ and CuTCNQ nano-garland (T5) (figure 3b). For pristine TCNQ, the characteristics principal vibrational modes appeared at 1205 cm^{-1} (C=CH bending), 1455 cm^{-1} (C-CN wing stretching), 1607 cm^{-1} (C=C ring stretching), and 2225 cm^{-1} (C≡N stretching) and commensurate well with literature.[16,24] In comparison to pristine TCNQ, the band corresponding to C-CN wing stretching was found to be shifted to 1374 cm^{-1} for CuTCNQ nano-garland.[16] The above observation could be attributed to reduction of TCNQ which further induced the formation CuTCNQ complexes. Additionally, the band related to C≡N stretching mode at 2208 cm^{-1} in CuTCNQ[24] was also observed to be shifted in comparison to the pristine TCNQ by 17 cm^{-1}. Such discernable differences confirm complete charge transfer between Cu and TCNQ and successful formation of CuTCNQ complexes.

Time dependent morphological evolution:

To have further insight into the formation mechanism of the hierarchy, time resolved experiments were also executed. Variation of CuTCNQ morphology for different growth times is

shown in FESEM images (figure 4). Inspection of micrograph (figure 4a) related to the sample for nominal growth time of 30 sec (T0) shows that the Cu nanowires become irregular, which are quite different from the bare one and growth initiates from very few places (inset of 4a). After 2 min, short CuTCNQ nanorods were found to grow radially over the Cu nanowire (T2) (figure 1b). With the small extension in growth time (5 minute), morphology of the hierarchy became more compact as more number of nanorods covered the Cu entire nanowire to form garland like architecture (T5) (figure 1d). Along with increase in number density of rods, the diameter and length of the nanorods were also found to increase in this case. Further elongation in growth time (30 min) leaded to changes in the dimension of the nanorods where the diameters of the nanorods became thicker as micron sized (T30) (figure 4b). Closer inspection (figure 4b inset) reveals that in such scenario nanorods aggregate to form thicker rods. Interestingly, prolonging the reaction time even further (60 min) resulted in micron sized CuTCNQ columnar structure (T60) where the top and side surface of these columns became rough due to partial dissolution (figure 4c and its inset).

Growth Mechanism:

We propose a plausible growth mechanism for the CuTCNQ hierarchy based on observed temporal growth behavior and it is schematically shown in figure 5. In general, pristine TNCQ, an excellent electron acceptor,[25] upon interacting with the electron donor Cu, forms blue color direct oxidation-reduction reaction between Cu and TCNQ occurs immediately after the dipping in acetonitrile solution which can be described as follows:

$$Cu^0 + TCNQ^0 \rightarrow Cu^+ TCNQ^-$$

The rough and uneven surfaces of the Cu nanowires along with very few short CuTCNQ nanorods over them signify the growth initiates from the nucleation site (T0). At this stage, TCNQ molecule directly adsorbs over the Cu nanowire. Once CuTCNQ complex is formed over the surface, the diffusion of TCNQ and copper towards the nucleation site prompts the kinetically control 1D growth. Again, owing to redox potential difference between Cu and TCNQ, electron from Cu transfers to adsorbed TCNQ through these CuTCNQ nanorods. Furthermore, due to chemical potential difference of Cu at top and bottom end of CuTCNQ nanorods, Cu^{+} ions migrate along the nanorods to combine with $TCNQ^{-}$ and results in CuTCNQ formation and thereby providing overall dimensional increment.[26] Such reasoning is analogous to our observed results. In T2, more number of CuTCNQ nanorods covered Cu nanowire than previous sample and for further elongation in time (T5), the hierarchies becomes densely packed and the average dimension of the rods also increases. Growth of these nanorods can proceed until complete depletion of any of the reactants (TCNQ or Cu).[27] As time prolongs (T30), higher dimensional and close packed CuTCNQ nanorods start to coalesce with the neighbors and quickly evolve into micron sized columnar structure.[23,28] It is well accepted that CuTCNQ has partial solubility in acetonitrile solution.[28] Thus during the total reaction span, competition between crystal growth and dissolution of the as grown nanostructure in the solution continues.[28,29] For small growth period, the dissolution is largely overshadowed by the substantial crystal growth but due to lack of reactant in the end (1h), the growth becomes moot and part of CuTCNQ start to dissolve in the solvent (figure 4d). XRD patterns of these samples support our proposed mechanism. Interestingly, traces of metallic Cu were detected up to the sample corresponding to 30min growth period and the Cu content was observed to decrease with increase in reaction time. For 1h sample, metallic Cu related peak completely vanished which

confirms absence of reactant. Additionally, the XRD patterns and Raman spectrum of all these samples (fig.6a, b) also confirm phase purity as no impurity related peaks were found to be present. In XRD patterns the star marked peaked designate the peak related to cu.

Field emission:

As per the common notion, numerous protruding branches of hierarchical nanostructure are propitious for enhancing field electron emission efficiency. A typical plot of field emission electron emission current density (J) as a function of electric field strength (E) for such hierarchical samples is presented in figure 7a, which reflects the remarkable influence of morphology on emission characteristics. The above demonstrates that the current density corresponding to T2 sample is highest for a given electric field. The turn-on fields, defined as macroscopic field required to draw an emission current density of 10 μA cm^{-2}, were found to be 2.69, 3.20, 7.37 and 8.30 Vμm^{-1} for T2, T5, T30 and T60 respectively. The emission current density attained the value of 1 mA cm^{-2}, known as the threshold field at 6.11 and 8.20 Vμm^{-1} for T2 and T5 samples. In contrast, other samples struggled to achieve the threshold value within the investigated range of electric fields. Field emission, being a quantum mechanical electron tunneling phenomenon from cathode to anode through vacuum, can be explained on the basis of Fowler Nordheim (FN) equation. According to this theory, field emission current density (J) is related with the applied field (E) via this equation: $J = (A\beta^2 E^2 / \phi)\exp(-B\phi^{3/2} / \beta E)$ Here A and B are constants with values 1.56×10^{-10} ($AV^{-2}eV$) and 6.83×10^{3} ($VeV^{-3/2}\mu m^{-1}$) respectively, $E = V/d$ (d is the anode-emitter distance), 'ϕ' is the work function of the emitting material which is 2.77 eV for CuTCNQ[18] and "β" is the geometrical field enhancement factor that enumerates the electric field amplification ability of the emitter at the emitting site. Field

enhancement factors (β), assessed from slopes of F–N plots (the linear $\ln(J/E^2)$ vs.1/E curves) are presented in figure 7b. Such linearity of these plots in high field region suggests the emission current necessarily originates only from barrier-tunneling electrons. The estimated β values from the curves were found to be 2366 and 2201 for T2 and T5. To judge the figure of merit of the novel organic hierarchy, we carefully surveyed the field values of various reported field emitters (both organic and inorganic) till date and tabulated them in Table S1† (see supporting information†). Additionally, we have also studied FE properties of the T2 sample at different anode-emitter separation (d) by varying d in the range of 80-120 μm with an interval of 20 μm. Interestingly, with the increments of d, the turn on fields were found to decrease linearly from 2.69 to 1.95 V μm^{-1} and threshold field values were found to downshift to 6.11 to 5.60V μm^{-1} (figure 7c).

Generally, field emission and thereby field enhancement factor is directly related to emitter geometry (such as aspect ratio, emitter tip sharpness etc.), neighbor emitter cross-talking (function of inter-emitter distance), work functions and vacuum gaps etc.[30,31] For quantitative analysis of the FE behavior, we will consider three most prominent factors: work function, emitter aspect ratio and emitter density within a specified area thereby field screening in the following discussion. Now, it is obvious that emitters possessing the lowest work function benefit the electron emission most. [18,32] For the current case, the low work function of CuTCNQ is certainly beneficial for betterment of high FE performance, but this aspect cannot explain the observed differences. So the performance discerning factors must be emitter geometry and the compactness of emitter thereby screening of electric field, as all other parameters remain identical for all samples. Higher nanowire coverage is usually expected to boost field emission performance owing to higher emitter tip density but very high density should lead to lower

performance due to higher field screening. Due to exponential dependence of inter-emitter distances, field screening has a much stronger influence of the field enhancement factor than other factors.[18] Thus, from field emission performance point of view, emitters with optimal tip separation are necessary for dodging the negative influence of field screening. Observed high emission performance shown by T2 sample may be accredited to hierarchical geometry where the nanorods tips are separated from each other considerably; hence field screening does not adversely affect electron emission performance by a great degree. Though the high structural aspect (aspect ratio) of individual emitter and more number of emitter sites in T5 are favorable for high emission performances but in practical scenario, it is found to render moderate β value as high emitter density ensued in high field screening which limits its FE performances. On the other hand, field emission performance of T5 was found to be better than T30 and T60 due to having large aspect ratio nanorods with higher coverage over Cu backbone. Lastly, inter electrode separation dependence of field emission behavior as observed in our case is similar to other documented reports.[33-35] With increased electrode distance, the effective emission area increases and more number of electrons can reach to the collector which results in increased current density.

Emission current stability is a decisive criterion for a good field emitter as undisrupted long term operation is a necessity in practical applications. To address this issue, we have studied the temporal variation of the emission currents for 120 min, starting with emission current of 1 mA cm^{-2} for T2 sample. Like other organic material based cold cathodes,[36,37] though the inevitable degradation in current density at initial stage could not be avoided for the present system, but the current remained almost constant thereafter. Only 3% maximum current fluctuation was registered in the later part. Fluctuation in emission stability due to resistive heating can be offset

by the special geometry of the hierarchy, where nanorods assembly provides high accessible surface area that enable good heat dissipation through radiation. Such nominal fluctuation highlights their high durability and fulfills all criteria of excellent field emitter.

To further verify our observed FE behavior, we computationally investigated the local electric field profile of T2 and T5 samples by finite element method using 'ANSYS Maxwell simulation package'. Though it is very much difficult to replicate the exact model of the observed morphology, yet we choose the simulation parameters in such way that they maintain direct analogy with the experimental morphology. 2-dimensional models, as used for theoretical investigation, comprising of very high density and high aspect ratio nanorods corresponding to T5 sample and the same for T2 sample, bearing sparse distribution of low aspect ratio nanorods are shown in figure 8a and 8b respectively. For both cases the separation between electrodes was kept fixed at 80 μm and a 2.2 KV potential was applied. For simulation purposes, bulk conductivity and dielectric constant values of CuTCNQ were $2.5x10^{-1}$ S cm^{-1} and 3 respectively[20,28] was used. A rainbow color co-ordinate was used to plot the electric field intensities in 2D plane where the blue and red color indicates the minimum and maximum field strength respectively. The plot clearly depicts local electric field distribution to be higher for T2 than T5 samples. From the above model, we calculated the maximum field values for T2 and T5 to be $3.12x10^7$ and $1.2x10^7$ respectively. As field enhancement factor (β) is defined as the ratio of maximum local field to applied macroscopic field; the ratio of field enhancement factor for T2 and T5 (i.e. β_{T2}/β_{T5}) can be directly estimated theoretically as $(E^m_{T2}/E_{T2})/(E^m_{T5}/E_{T5})$ where E^m_{T2}, E^m_{T5} and E_{T2}, E_{T5} are maximum local fields and applied macroscopic fields for T2 and T5 samples respectively. As we used $E_{T2} = E_{T5} = 2.2$ KV in our model, we directly evaluate $\beta_{T2}/\beta_{T5} = E^m_{T2}/E^m_{T5} \sim 2.6$; which is close to our experimental resulted ratio of 1.07.

Conclusion:

In summary, using simple synthesis protocols, we successfully prepared garland shaped novel 3-dimensional CuTCNQ hierarchy. Scalable amount of well crystalline products in single synthesis run signifies its technological importance. By controlling growth time, the morphology of the nanostructures was tuned and on the basis of the above, we also proposed a plausible growth mechanism. Field emission investigation revealed the optimized hierarchy possesses decently low turn on field of 2.69 $V\mu m^{-1}$ and high field enhancement factor of 2366 which are better or comparable with previously reported semiconductors. These novel nanostructures are hypothesized to be a valuable addition not only to the fundamental science but also to modern day electronic and optoelectronic devices.

Acknowledgement:

One of us, S.P. wishes to thank the Council of Scientific and Industrial Research (CSIR), Government of India., for awarding her Junior Research Fellowship (JRF) during the execution of the work. The authors also wish to acknowledge the University Grants Commission (UGC), the Govt. of India, for 'University with potential for Excellence (UPE II)' scheme.

Figure caption:

(1) FESEM images of Cu nanowires (a) T2 (b); CuTCNQ nano-garland (T5) in low magnification (c); (inset shows digital image of real garland) and high magnification (d).

(2) XRD patterns of the synthesized Cu nanowire, T2 and CuTCNQ nano-garland (a); the Cu 2p XPS spectrum(b); XPS spectrum of N 1s for CuTCNQ nano-garland (c).

(3) (a) FT-IR spectra and (b) Raman spectra of the pristine TNCQ and CuTCNQ nano-garland (T5) respectively.

(4) Morphological evolution with time (a) 30 sec, (b) 30 min and (c) 60 min. Insets exhibit the corresponding higher magnification images.

(5) Schematic showing the possible growth mechanism.

(6) XRD patterns (a) and Raman spectra (b) of the CuTCNQ hierarchies for different growth time (T0, T2, T5, T30 and T60) along with Cu nanowire and inset of (b) shows the Raman spectra intensity variation for different growth times.

(7) J–E plots corresponding to the samples under investigation (a); F–N plots for T2 and T5 and inset showing F–N plots for T0 and T2 (b); J-E plots of T2 sample for different vacuum gaps (c) and emission stability for T2 sample (d).

(8) Color mapping of the magnitude of electric field distribution for nano- hierarchy (T2) (a) and nano-garland (T5) (b).

Reference:

(1) H. Kim, S. Jeon, M. Lee, Junghan Lee and K. Yong, *J. Mater. Chem.*, 2011, **21**, 13458.

(2) U. N. Maiti, S. Maiti, N. S. Das and K. K. Chattopadhyay, *Nanoscale*, 2011, **3,** 4135.

(3) R. Yu, C. Zhang, Q. Meng, Z. Chen, H. Liu and Z. Guo, *ACS Appl. Mater. Inter.,* 2013, **5**, 12394.

(4) R. R. Devarapalli, D. R. Shinde, F. Barka-Bouaifel, S. G. Yenchalwar, R. Boukherroub, M. A. More and M. V. Shelke, *J. Mater. Chem.*, 2012, **22**, 22922.

(5) S. Maiti, U. N. Maiti, B. C. Behera, S. Pal and K. K. Chattopadhyay, *J. Mater. Chem. C*, 2013, **1**, 4940.

(6) R. Basori, K. Das, P. Kumar, K. S. Narayan, and A. K. Raychaudhuri, *Appl. Phys. Lett.*, 2013, **102**, 061111.

(7) K. Wang, X. Qian, L. Zhang, Y. Li, and H. Liu, *ACS Appl. Mater. Inter.,* 2013, **5**, 5825.

(8) S. Zhang, Z. Lu, L. Gu, L. Cai and X. Cao, *Nanotechnology*, 2013, **24**, 465202.

(9) F. Tian, W. Liu and C.- R. Wang, *J. Phys. Chem. C*, 2008, **112**, 8763.

(10) N. Gu, W. Lu, S. M. Pang, C. W. Yuan and Y. Wei, *Thin Solid Films*, 1994, **243**, 468.

(11) H. liu, J. Xu, Y. li and Y. li, *Acc. Chem. Res.*, 2010, **43**, 1496.

(12) S. Cui, H. Liu, L. Gan, Y. Li and D. Zhu, *Adv. Mater*., 2008, **20**, 2918.

(13) A. Pearson, A. P. O'Mullane, V. Bansal, and S. K. Bhargava, *Inorg. Chem.*, 2011, **50**, 1705.

(14) H. Liu, Z. Liu, X. Qian, Y. Guo, S. Cui, L. Sun, Y. Song, Y. Li and D. Zhu, *Cryst. Growth Des.,* 2010, **10**, 237.

(15) Y. Liu, L. Jiang, H. Dong, Z. Tang and W. Hu, *Small*, 2011, **7**, 1412.

(16) K. Zheng, X. Li, X. Mo, G. Chen, Z. Wang, and G. Chen, *Appl. Surf. Sci.*, 2010, **256**, 2764.

(17) H. Liu, X. Wu, L. Chi, D. Zhong, Q. Zhao, Y. Li, D. Yu, H. Fuchs and D. Zhu, *J. Phys. Chem. C*, 2008, **112**, 17625.

(18) S. Maiti, U. Narayan Maiti, S. Pal and K. K. Chattopadhyay, *Nanotechnology*, 2013, **24**, 465601

(19) M. Kevin, W. L. Ong, G. H. Lee and G. W. Ho, *Nanotechnology*, 2011, **22**, 235701.

(20) R. A. Heintz, H. Zhao, X. Ouyang, G. Grandinetti, J. Cowen, and K. R. Dunbar, *Inorg. Chem.*, 1999, **38**, 144.

(21) H. Liu, Q. Zhao, Y. Li, Y. Liu, F. Lu, J. Zhuang, S. Wang, L. Jiang, D. Zhu, D. Yu and L. Chi, *J. Am. Chem. Soc.*, 2005, **127** , 1120.

(22) K. Hiraishi, A. Masuhara, T. Yokoyama, H. Kasai, H. Nakanishi and H. Oikawa, *Jour. Cryst. Growth*, 2009, **311,** 948.

(23) Y. Liu, Z. Ji, Q. Tang, L. Jiang, H. Li, M. He, W. Hu, D. Zhang, L. Jiang, X. Wang, C. Wang, Y. Liu and D. Zhu, *Adv. Mater.*, 2005, **17**, 2953.

(24) P. G. Gucciardi, S. Trusso, C. Vasi, S. Patane` and M. Allegrini, *Phys. Chem. Chem. Phys.*, 2002, **4**, 2747.

(25) Z. M. Davoudi, A. E. Kandjani , A. I. Bhatt, I. L. Kyratzis, A. P. O'Mullane and V. Bansal, *Adv. Funct. Mater.,* 2013, DOI: 10.1002/adfm.,201302368.

(26) H.-X. Ji, J.-S. Hu, Y.-G Guo, W.-G. Song and L.-J. Wang, *Adv. Mater.,* 2008, **20**, 4879.

(27) K. Xiao, J. Tao, Z. Pan, A. A. Puretzky, I. N. Ivanov, S. J. Pennycook and D. B. Geohegan, *Angew. Chem.*, 2007, **119**, 2704.

(28) Y. Liu, H. Li, Z. Ji, Y. Kashimura, Q. Tang, K. Furukawa, K. Torimitsu, W. Hu and D. Zhu, *Micron*, 2007, **38**, 536.

(29) X.–H. Zhou, S.–J. Wei, and S.–S. Zhang, *Langmuir*, 2008, **24**, 4464.

(30) U. N. Maiti, S. Maiti, S. Goswami, D. Sarkar and Kalyan K. Chattopadhyay, *CrystEngComm.*, 2011, **13**, 1976.

(31) U. N. Maiti, S. Maiti, T. P. Majumder and K. K. Chattopadhyay, *Nanotechnology*, 2011, **22**, 505703.

(32) S. Cui, Y. Li, Y. Guo, H. Liu, Y. Song, J. Xu, J. Lv, M. Zhu and D. Zhu, *Adv. Mater.*, 2008, **20**, 309.

(33) M. Sun, Y. Gao, C. Zhi, Y. Bando and D. Golberg, *Nanotechnology*, 2011, **22**, 145705.

(34) A. Khademi, R. Azimirad, A. A. Zavarian and A. Z. Moshfegh, *J. Phys. Chem. C*, 2009, **113**, 19298.

(35) M. Hafeez, T. Zhai, A. S. Bhatti, Y. Bando and D. Golberg, *J. Phys. Chem. C*, 2012, **116**, 8297.

(36) I. Musa, D. A. I. Munindrasdasa, G. A. J. Amaratunga and W. Eccleston, *Nature*, 1998, **395**, 362.

(37) J.-J. Chiu, C.-C. Kei, T.-P. Perng and W.-S. Wang, *Adv. Mater.*, 2003, **15**, 1361.

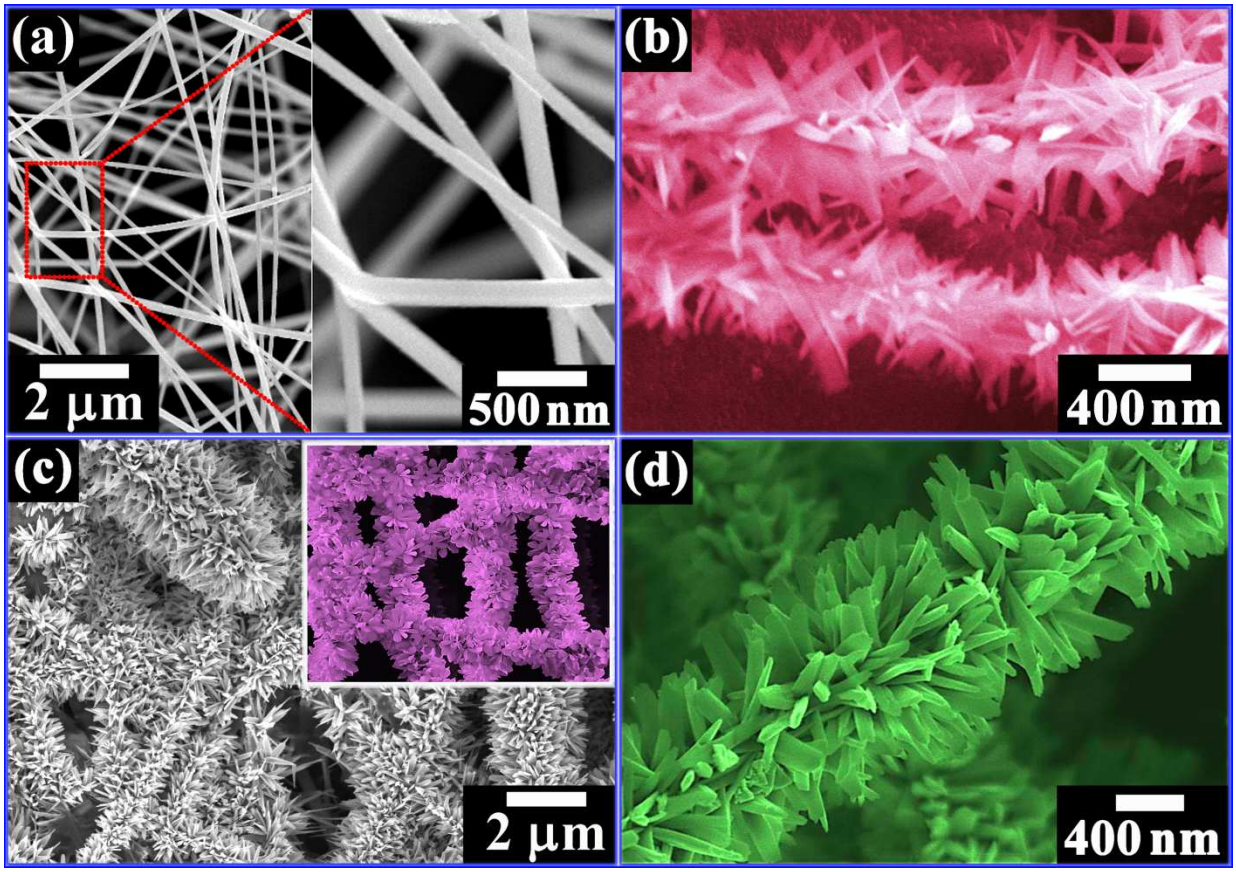

Fig.1 Pal et al.

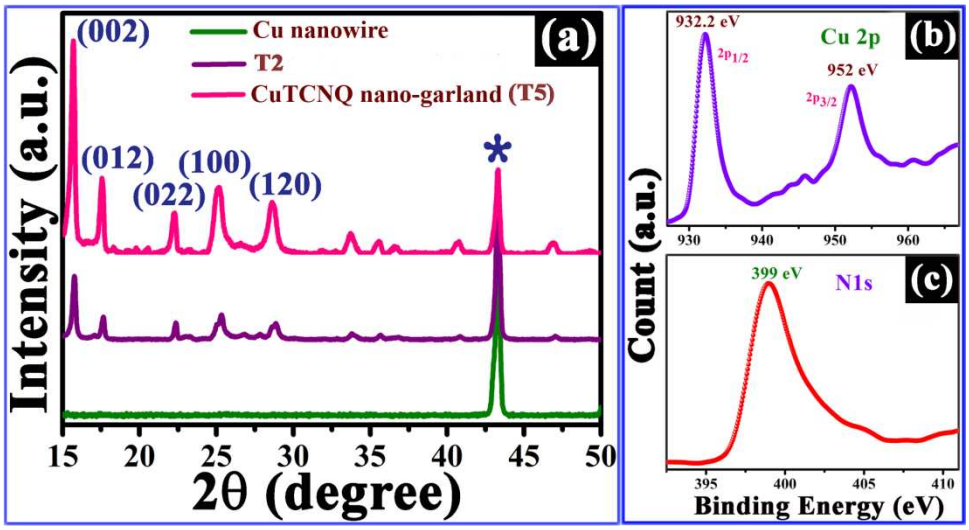

Fig.2 Pal et al.

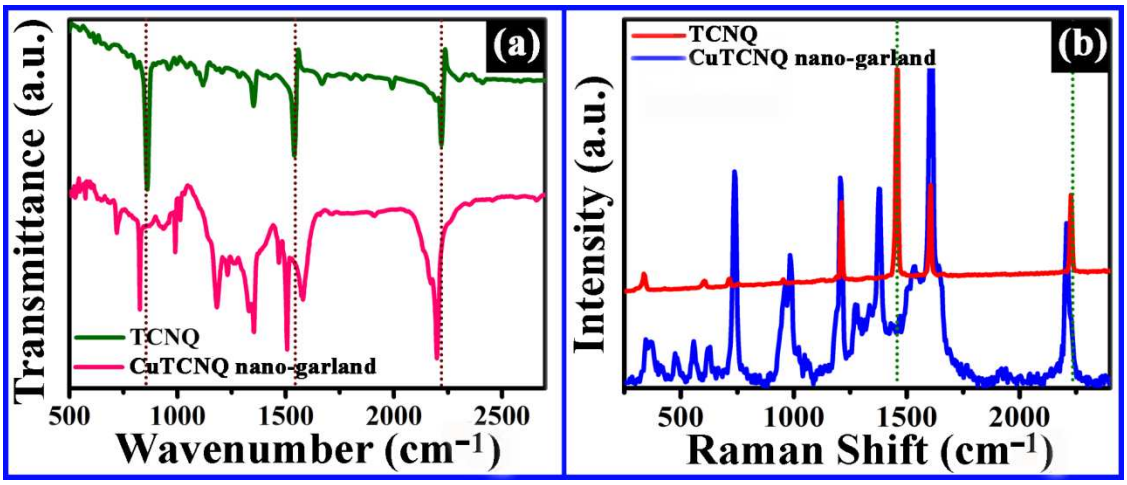

Fig.3 Pal et al.

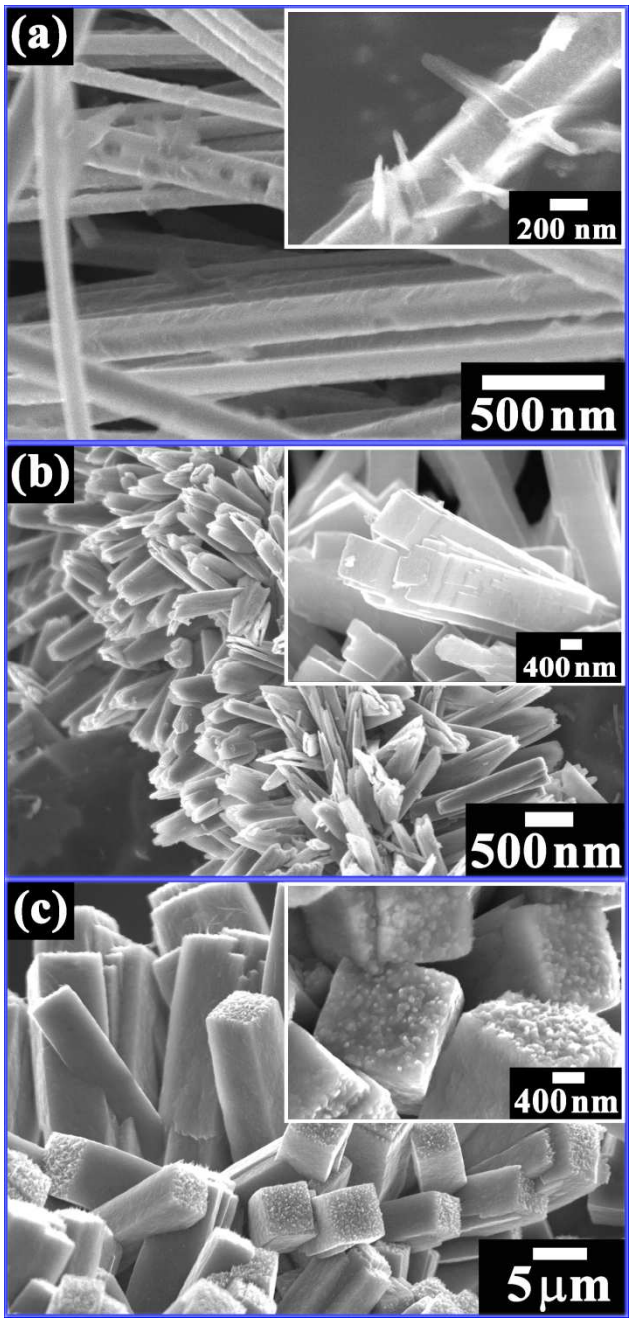

Fig.4 Pal et al.

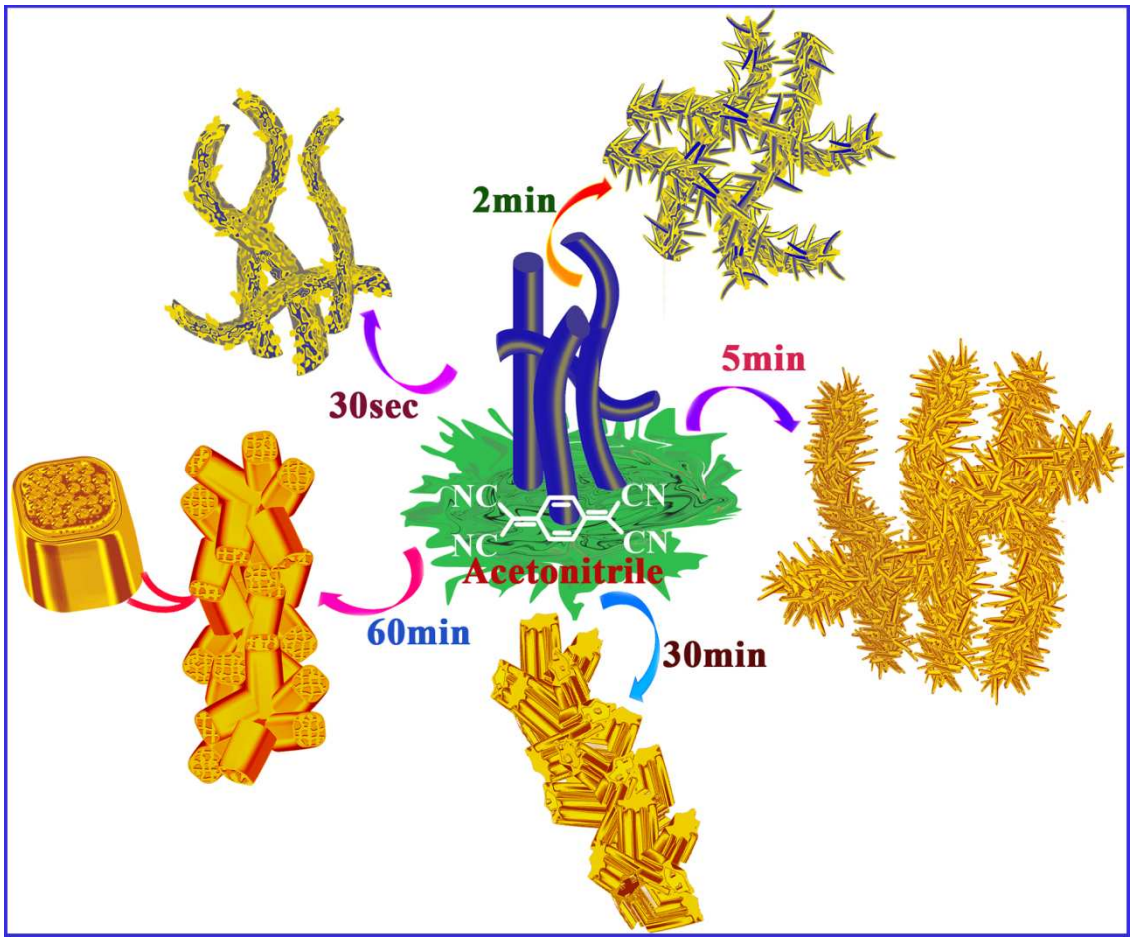

Fig.5 Pal et al.

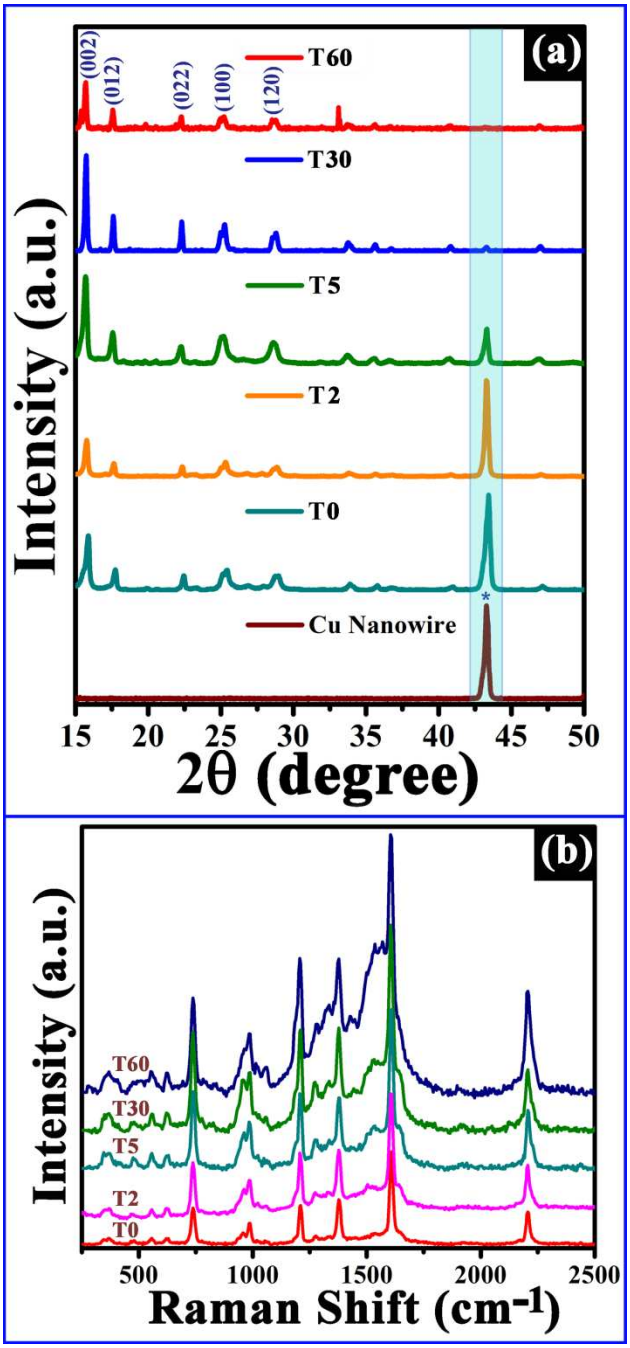

Fig.6 Pal et al.

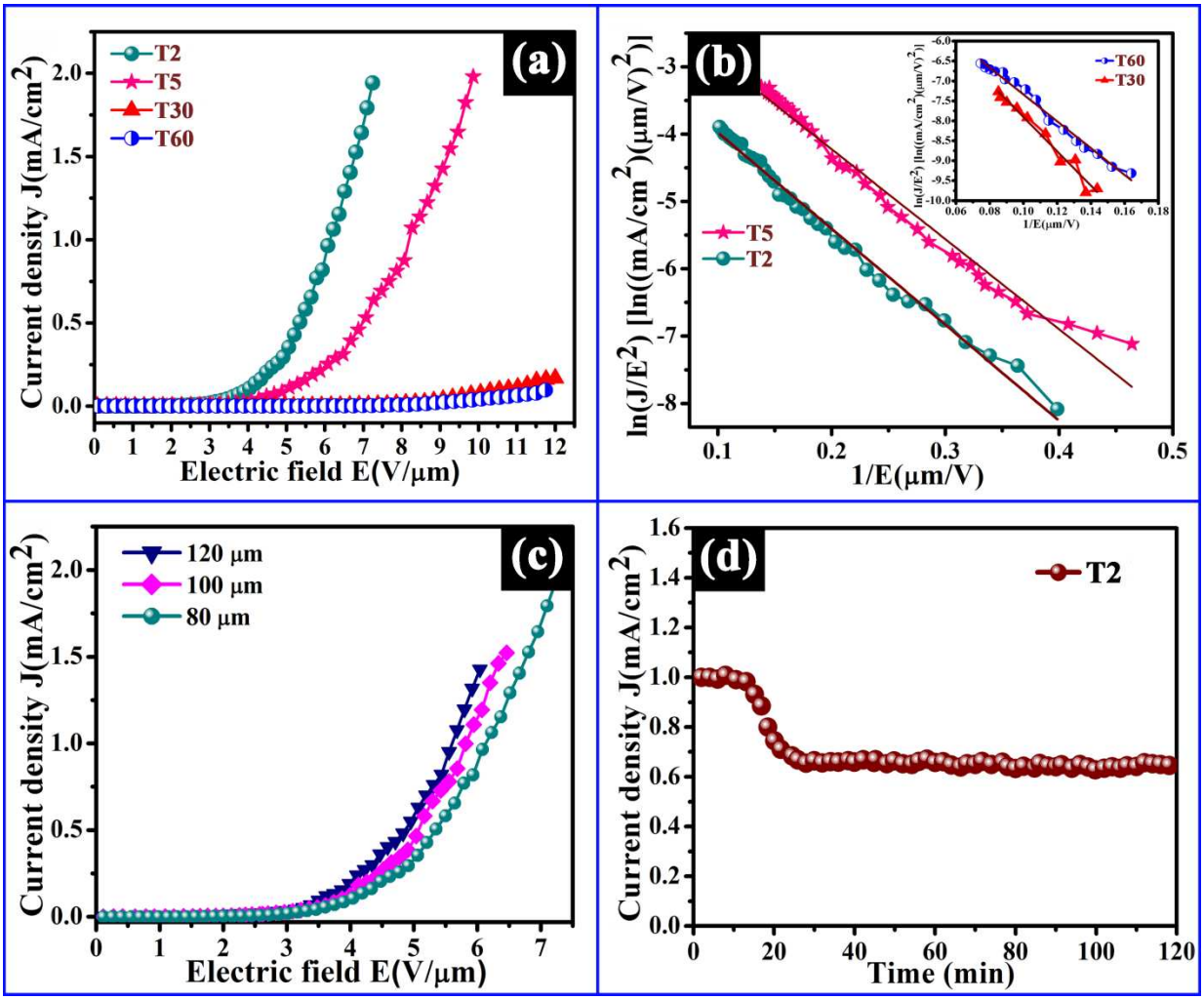

Fig.7 Pal et al.

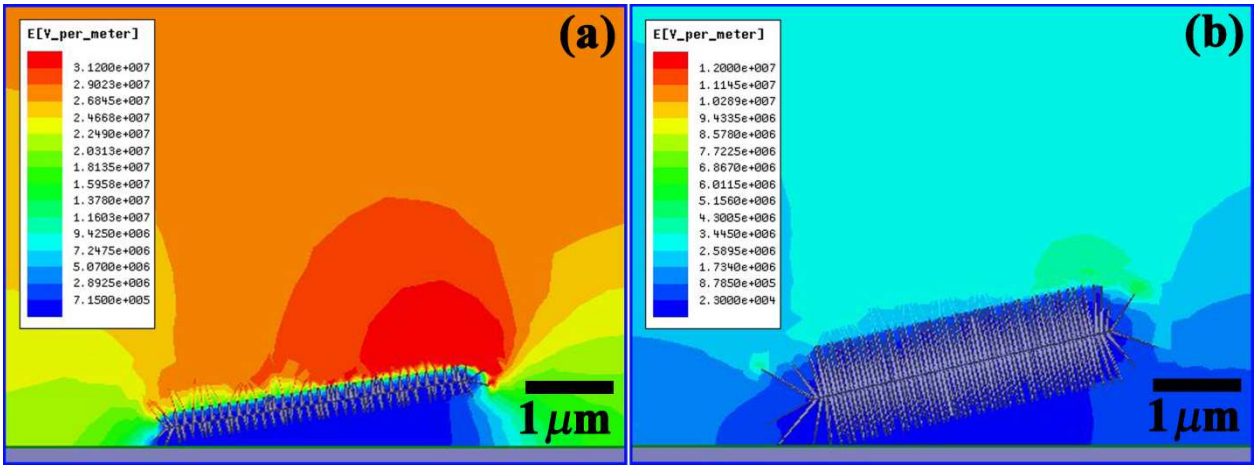

Fig.8 Pal et al.

Table of Content:

Scalable approach for the realization of garland shaped 3D assembly of CuTCNQ nanorods: efficient electron emitter

Shreyasi Pal[a], Soumen Maiti[a], Uday Narayan Maiti[b], and Kalyan Kumar Chattopadhyay[a*]

[a]Thin Films and Nanoscience Laboratory, Department of Physics, Jadavpur University, Kolkata 700032, India, [b] KAIST, South Korea.

[*]Corresponding Author: Email: kalyan_chattopadhyay@yahoo.com

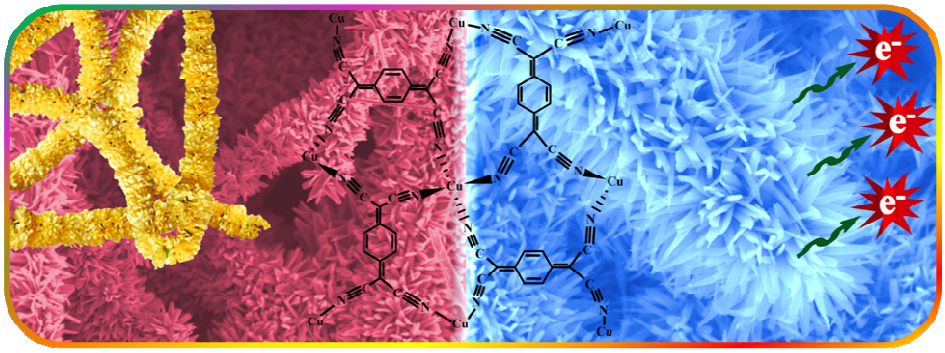

Garland shaped CuTCNQ nano-architecture was realized over Cu nanowire and corresponding growth mechanism was elucidated by monitoring structural evolution of intermediate products. These hierarchies with branched assemblies of nanorods exhibit excellent electron emission performances.